

Observation of Selective Plasmon-Exciton Coupling in Nonradiative Energy Transfer: Donor-Selective versus Acceptor-Selective Plexcitons

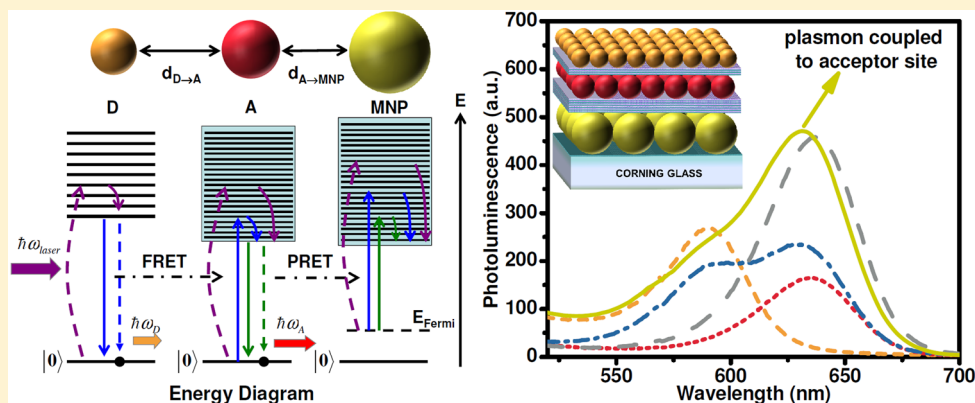
Tuncay Ozel,^{§,||} Pedro Ludwig Hernandez-Martinez,^{†,‡,§,||} Evren Mutlugun,^{†,‡,§} Onur Akin,[§] Sedat Nizamoglu,[§] Ilkem Ozge Ozel,[§] Qing Zhang,[‡] Qihua Xiong,^{*,‡} and Hilmi Volkan Demir^{*,†,‡,§}

[†]Center of Excellence for Semiconductor Lighting and Displays, School of Electrical and Electronic Engineering, Nanyang Technological University, LUMINOUS! Singapore 639798

[‡]Division of Physics and Applied Physics, School of Physical and Mathematical Sciences, Nanyang Technological University, 21 Nanyang Link, Singapore 637371

[§]Department of Physics, Department of Electrical and Electronics Engineering, and UNAM – Institute of Materials Science and Nanotechnology, Bilkent University, TR-06800, Ankara, Turkey

S Supporting Information



ABSTRACT: We report selectively plasmon-mediated nonradiative energy transfer between quantum dot (QD) emitters interacting with each other via Förster-type resonance energy transfer (FRET) under controlled plasmon coupling either to only the donor QDs (i.e., donor-selective) or to only the acceptor QDs (i.e., acceptor-selective). Using layer-by-layer assembled colloidal QD nanocrystal solids with metal nanoparticles integrated at carefully designed spacing, we demonstrate the ability to enable/disable the coupled plasmon-exciton (plexciton) formation distinctly at the donor (exciton departing) site or at the acceptor (exciton feeding) site of our choice, while not hindering the donor exciton-acceptor exciton interaction but refraining from simultaneous coupling to both sites of the donor and the acceptor in the FRET process. In the case of donor-selective plexciton, we observed a substantial shortening in the donor QD lifetime from 1.33 to 0.29 ns as a result of plasmon-coupling to the donors and the FRET-assisted exciton transfer from the donors to the acceptors, both of which shorten the donor lifetime. This consequently enhanced the acceptor emission by a factor of 1.93. On the other hand, in the complementary case of acceptor-selective plexciton we observed a 2.70-fold emission enhancement in the acceptor QDs, larger than the acceptor emission enhancement of the donor-selective plexciton, as a result of the combined effects of the acceptor plasmon coupling and the FRET-assisted exciton feeding. Here we present the comparative results of theoretical modeling of the donor- and acceptor-selective plexcitons of nonradiative energy transfer developed here for the first time, which are in excellent agreement with the systematic experimental characterization. Such an ability to modify and control energy transfer through mastering plexcitons is of fundamental importance, opening up new applications for quantum dot embedded plexciton devices along with the development of new techniques in FRET-based fluorescence microscopy.

KEYWORDS: Localized plasmons, nonradiative energy transfer, excitons, metal nanoparticles, semiconductor quantum dots, plexcitons, layer-by-layer assembly

The Förster-type resonance energy transfer (FRET), an important proximity effect that can strongly modify the emission kinetics of fluorophores serving as donors and acceptors, is widely used in biotechnology especially as

Received: March 11, 2013

Revised: June 5, 2013

Published: June 11, 2013

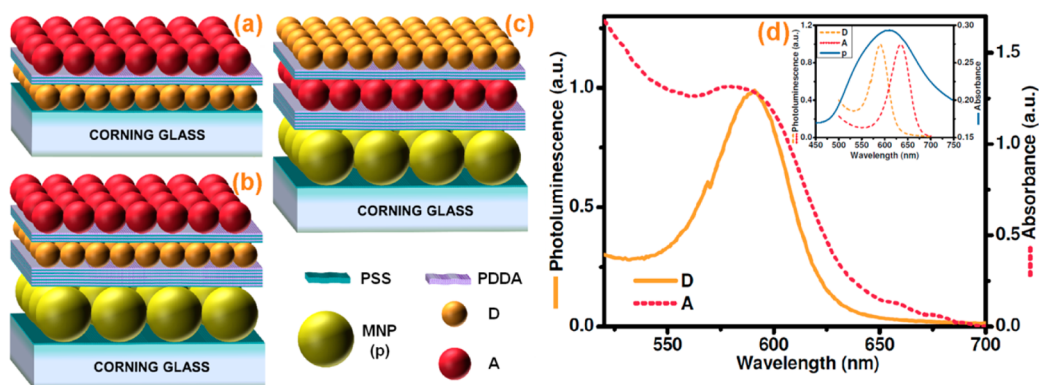


Figure 1. Layered architectures of (a) conventional FRET, (b) plasmon-mediated FRET (PM-FRET) with plasmon coupling only to the donor quantum dots (where the plasmonic interaction with the acceptors is intentionally prevented), and (c) complementary PM-FRET with plasmon coupling only to the acceptor quantum dots (while deliberately avoiding the plasmonic interaction with the donors). (d) Photoluminescence spectrum of the donor quantum dots given with the optical absorption spectrum of the acceptor quantum dots and (inset) photoluminescence spectrum of both of the quantum dots given with the absorption spectrum of the Au nanoparticle film.

nanorulers and biosensors and in nanophotonics for light generation and light-harvesting applications.^{1–6} Among the colloidal semiconductor quantum dots (QDs), also known as nanocrystals (NCs), FRET can also take place by means of the excitation energy of the donor QDs that is nonradiatively transferred to the acceptor QDs, through the long-range intermolecular dipole–dipole coupling of the donor QD emission to the excitation of the acceptor QD. In addition to FRET, another proximity mechanism of fundamental interest is the plasmon resonance energy transfer (PRET), for example, effective among semiconductor QDs and metal nanoparticles (MNPs), through which the emission characteristics of excited QDs is altered via localized electric fields created by plasmonic oscillations. One favored result of this mechanism is the spontaneous emission enhancement of QDs in the controllably close vicinity of MNPs with the generation of plasmonic emitters also known as plasmaphores.^{6–10}

Most recently, the combination of these two fundamental energy transfer mechanisms has gained a strong interest, and increased FRET rates between donor–acceptor pairs of various fluorophores under plasmon coupling has been recently reported.^{11–17} Lunz et al. have successfully demonstrated increased Förster radius with the aid of simultaneously plasmon-coupling the donor–acceptor pair, which is important for expanding effectively the interaction volume through the intermediate use of plasmons.¹⁶ In these recent reports, both the donor and the acceptor fluorophores were plasmon-coupled at the same time either by using a layer of metal nanostructures or a thin layer of metal sandwiched by the donor and acceptor layers; or the donors and acceptors were initially blended and placed directly on top of a metal layer. However, in all of these previous systems the excitonic interaction directly between the donor and the acceptor was blocked, and the coupled plasmon–exciton, also known as plexciton,^{17–20} of the donor and that of the acceptor have thus far remained unclear within the resulting coupled energy transfer mechanisms because the plasmon coupling was not controlled to take place distinctly either at the donor site or the acceptor site, but at both sides at the same time. To date, there has been no report focusing on the independent control of the plasmon coupling to the donor and that to the acceptor individually in a cascaded energy transfer mechanism.

Here, we demonstrate the first account of cascaded plasmonic and nonradiative energy transfer interactions that are controlled by selectively generating plexciton either at only the donor QDs or at only the acceptor QDs of the energy transfer pairs using layered constructs of MNPs and QDs. This allows for the gentle modification of one member of the FRET pair through plasmonics, while the pair still sustains exciton transfer directly between them, unlike the previous studies that completely destroy direct donor exciton–acceptor exciton coupling but instead rely on donor exciton–metal plasmon and metal plasmon–acceptor exciton coupling. The current approach uniquely provides the ability to master and understand the plexciton interactions occurring at the initial (donor) site or the final (acceptor) site of the energy transfer, which leads to fundamental differences in terms of optical emission properties of the FRET pair. We analyze the consequent modifications in QD emission kinetics under plasmon-coupled FRET conditions and systematically investigate the cascaded energy transfer mechanisms through steady state and time-resolved photoluminescence measurements, along with lifetime and decay rate analyses. Also, here we propose and develop a theoretical model to understand and explain the experimental results. Both experimentally and theoretically, we show that cascading FRET after PRET is not the same as cascading PRET after FRET, which means that the cascading order does actually matter.

In this work, Au MNPs of 15 nm in diameter are synthesized following a similar synthesis procedure described by Enustun et al.²¹ Donor and acceptor CdTe QDs are prepared following the synthesis procedure of Gaponik et al.²² to obtain sufficient spectral overlaps with the plasmon resonance spectrum of Au MNPs to a desired extent, depending on the investigated plasmon coupling mechanism. Monolayer films of QDs and MNPs, and separating dielectrics between them, are assembled in subnanometer precision through layer-by-layer (LbL) assembly technique using oppositely charged polyelectrolyte polymers.²³ Synthesis and assembly procedures are explained in detail in our previous works.^{5,8}

The plexciton interaction is structurally controlled by design through placing the plasmonic layer in the proximity of the donors (for strong donor–exciton plasmon-coupling) while sufficiently being far away from the acceptors (for weak acceptor–exciton plasmon-coupling), or vice versa. Corning

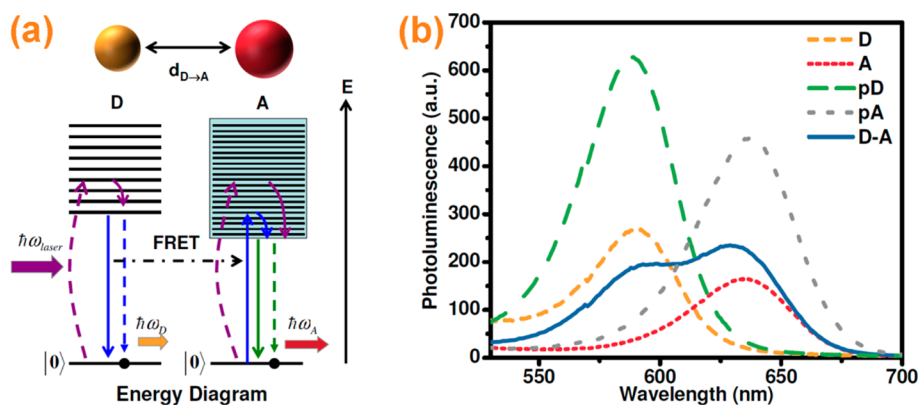


Figure 2. (a) Schematic representation of the energy band diagram with the absorption process of the donor/acceptor, fast relaxation process, light emission process, energy transfer from the donor to the acceptor and the Coulomb interaction between the D–A pair. (b) Photoluminescence (PL) spectra of the D (dotted orange), A (dotted red), plasmon-coupled D (dashed green), and plasmon-coupled A (dashed gray). D–A QD pair (solid blue) under Förster-type energy transfer.

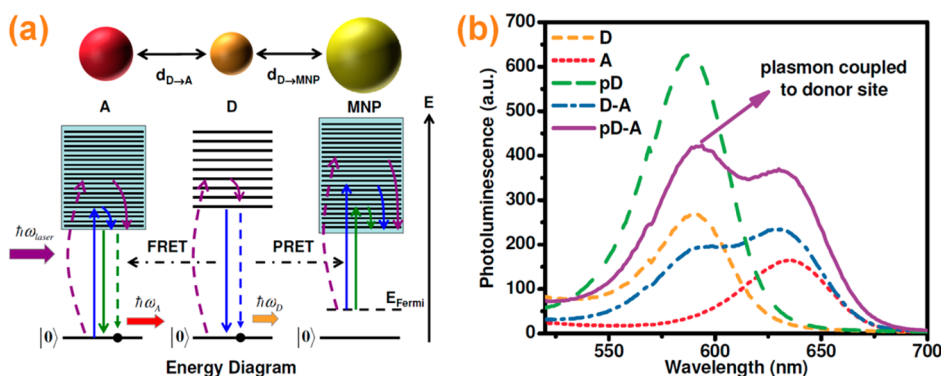


Figure 3. (a) Schematic representation of a donor–acceptor (D–A) energy transfer pair in the case of plasmon coupling to only donor QD along with an energy band diagram in which the absorption process of the MNP/donor/acceptor, fast relaxation process, light emission process, energy transfer from the donor to the acceptor and the Coulomb interaction between the donor and acceptor pairs are shown. In the energy diagram, the discrete energy levels for the QDs are depicted, as well as the energy level for the localized plasmons within the continuous energy band of the MNP. (b) Photoluminescence (PL) spectra of the D (dotted orange), A (dotted red), D–A QD pair (dashed blue) under Förster-type energy transfer, plasmon-coupled D (dashed green), and FRET for the D–A QD pair when only the donor QD is coupled to MNP (solid magenta).

glass surfaces are pretreated by successive deposition of 6 monolayers (MLs) of positively charged poly-(diallyldimethylammoniumchloride) (PDDA) and negatively charged poly(styrene sulfonate) (PSS) separator film pair prior to the deposition of QDs for homogeneous assembly. For the control group of only FRET, we first prepare a sample in the absence of plasmonic structures to benchmark the conventional FRET mechanism between the donor (D) and acceptor (A) QD layer. In this sample, 1 ML of the donor QD is separated from 1 ML of the acceptor QD by consecutive deposition of 3 MLs of dielectric PDDA/PSS film pair (each ML corresponding to 1.1 ± 0.2 nm) as schematically illustrated in Figure 1a (dubbed as D–A in the following figures). In one set of the control groups for plasmonics, the acceptor QDs are plasmon-coupled by the use of 6 MLs of Au MNPs separated by 6 MLs of PDDA/PSS pair and finally followed by 1 ML of the acceptor QDs (pA). Similarly, another set (pD) is prepared for plasmon coupling to the donor. Here, in order to obtain plasmon-enhanced QD emission, as opposed to quenching, the separation between the QD layer and MNP layers is optimized. In the case of too short distance between semiconductor QDs and metal MNPs, the emission is quenched due to increased nonradiative processes. Also, in the case of too large separation between QDs and MNPs, the local electric field generated by

MNPs vanishes and, thus, does not affect the photoluminescence kinetics of QDs. Emission enhancement can be achieved in a separation range of 2–20 nm (including surfactants and ligands).^{24–26} Our spacer optimization results show that the strongest emission enhancement is observed in the presence of 6 MLs of PDDA and PSS in successive deposition.

Next, we repeat the first FRET experiment with the use of plasmon-coupled donor QDs to generate donor-selective plexitons. Plasmon-coupled donor QD layer is separated by 3 MLs of PDDA/PSS pair and 1 ML of acceptor QD film layer is deposited on the top (thus pD–A as shown in Figure 1b). Subsequently, we repeat the first FRET experiment also by using plasmon-coupled acceptor QD film layer, this time to create acceptor-selective plexiton. In this case, the plasmon-coupled acceptor QD layer is separated by 3 MLs of PDDA/PSS pair and 1 ML of donor QD layer is deposited on the top (hence D–pA as given in Figure 1c in reverse order). In all these sets, we deposit 6 MLs of Au MNPs to generate strong plasmon modes and obtain a plasmon resonance spectrum that spans a wide range of visible wavelengths matching donor and acceptor spectra. A strong spectral overlap between the absorption of the acceptor QDs and the emission of the donor QDs is observed as depicted in Figure 1d, as needs to be

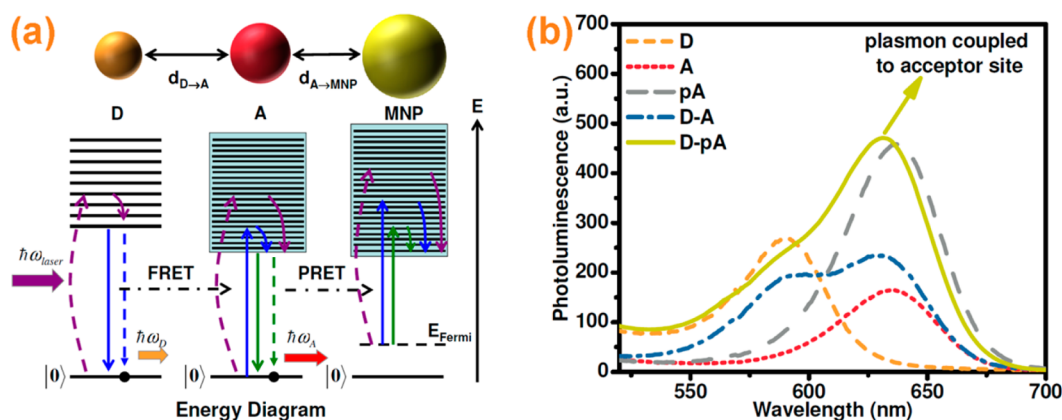


Figure 4. (a) Schematic representation of a donor–acceptor (D–A) energy transfer pair in the case of plasmon coupling to only acceptor QD along with an energy band diagram with the absorption process of the MNP/donorQD/acceptorQD, fast relaxation process, light emission process, energy transfer from the donor to the acceptor and the Coulomb interaction between the donor and acceptor pairs are shown. In the energy diagram, the discrete energy levels for the QDs are depicted, as well as the energy level for the localized plasmons within the continuous energy band of the MNP. (b) Photoluminescence (PL) spectra of the D (dotted orange), A (dotted red), D–A QD pair (dashed blue) under Förster-type energy transfer, plasmon-coupled A (dashed gray), and FRET for the D–A QD pair when only the acceptor QD is coupled to MNP (solid yellow).

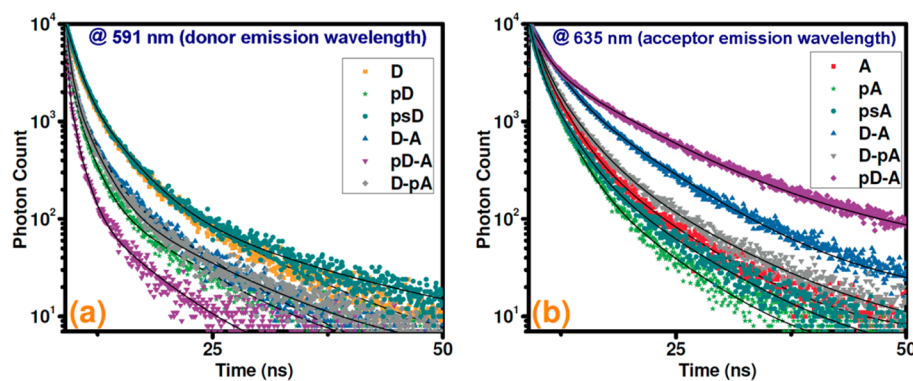


Figure 5. Time-resolved photoluminescence decay curves (using a three-exponential decay model) of the quantum dots under different plasmonic and/or FRET conditions collected at (a) the donor emission wavelength (591 nm) and (b) the acceptor emission wavelength (635 nm).

satisfied for FRET condition. Also, the donor and acceptor QDs are located in the range of Förster radius by considering the separation due to surfactants/ligands around QDs and the dielectric spacer layer between them. We used only one monolayer of QDs in our experiments since there is an additional energy transfer between each monolayer in the presence of a few QD layers, and also the separation between MNPs and each QD layer in the structure is different, which would complicate the understanding of emission and energy transfer mechanisms.

Following steady-state photoluminescence spectroscopy of D–A, pD–A, and D–pA presented in Figures 2–4, respectively, a comparative study of the emission kinetics of the nanocomposite constructions is conducted using time-resolved fluorescence, as depicted in Figure 5a,b, which is a clear evidence of strong modification caused by plasmon and/or FRET coupling. Fluorescence lifetimes are measured using a time-correlated single photon counting system (Picoquant-FluoTime200) with 16 ps resolution with an excitation laser at 375 nm. To model the decay curves and evaluate the amplitude averaged lifetimes, the data are fit with multiexponentials using deconvolution of the instrument response function (Fluo-fit decay analysis software by PicoQuant Technologies, Germany).

Donor–Acceptor FRET System. In conventional FRET sample, the acceptor emission is enhanced while the donor

emission is suppressed simultaneously as depicted in Figure 2b. We observe a 1.30-fold emission enhancement of the acceptor QDs owing to FRET. Using the time-resolved fluorescence decay fit parameters, we compute FRET rates between the donor and acceptor QDs and also the FRET efficiency of the prepared samples. Amplitude averaged photoluminescence lifetime of the donor QDs decreases from 1.33 to 0.62 ns, while the lifetime of the acceptor QDs increases from 1.53 to 3.11 ns as shown in Figure 5a (orange square, blue triangle-up, respectively) and Figure 5b (red square, blue triangle-up, respectively). These photoluminescence decay lifetime modifications provide evidence for strong energy transfer between the donor and acceptor QDs. For the first system described here, we calculate the energy transfer rate to be 0.86 ns^{-1} and the FRET efficiency to be 0.53.

In the case of FRET in D–A QD pairs (as in Figure 2a), the emission enhancement factor for the donor and acceptor is given by (details are in Supporting Information: FRET in QDs pair)

$$\kappa_{D,NRET} = \frac{\gamma_{D,exc}}{\gamma_{D,exc} + \gamma_{NRET}} \quad (1)$$

$$\kappa_{A,NRET} = 1 + \frac{\gamma_{A,exc}}{\gamma_{A,exc} + \gamma_{NRET}} \quad (2)$$

where $\gamma_{D(A),exc}$ is the exciton recombination rate of the donor (acceptor) and $\gamma_{NRET} = \gamma_{D,exc}(R_0/r)^6$ is the Förster-type D–A transfer rate. Here, R_0 is the Förster radius,²⁷ and r is the separation distance between the D and the A. Parameters used in these calculations are provided in the Supporting Information: Numerical Results.

For the case of D–A QD pair with FRET (no plasmonic effects in play) (Figure 2b, solid blue line), we obtain an emission enhancement factor for the acceptor QDs of 1.46, which is comparable to the experimental value of 1.30. In addition, there is a 35% reduction in the photoluminescence (PL) intensity of the donor QDs.

Plasmon Coupled Donor (Acceptor) System. We further employed plasmonic coupling to either donor or acceptor quantum dots using Au metal nanoparticles. The emission enhancement factor ($\kappa_{PM}(\omega)$) for the QD in the presence of MNP is

$$\kappa_{PM}(\omega_{emiss}, \omega_{laser}) = \frac{A(\omega_{emiss})A(\omega_{laser})\gamma_{0,exc}}{A(\omega_{emiss})Y_0\gamma_{0,exc} + (1 - Y_0)\gamma_{0,exc} + \gamma_{nr,metal}} \quad (3)$$

where $\gamma_r = A(\omega_{emiss})\gamma_{0,r}$, $\gamma_{nr} = \gamma_{0,nr}$ are the radiative and nonradiative rate of QDs in the presence of MNPs, respectively.²⁸ With $\gamma_{0,r} = Y_0\gamma_{0,exc}$, $\gamma_{0,nr} = (1 - Y_0)\gamma_{0,exc}$ is the exciton recombination rate in the absence of MNP and Y_0 is the quantum yield for the QD. Here $\omega_{emiss}(\omega_{laser})$ are the exciton emission (excitation laser) frequencies and $A(\omega)$ is the electric field enhancement factor,²⁸ which is defined as

$$A(\omega) = \frac{\int_{SQD} |E_{in,QD}|^2 dV}{\int_{SQD} |E_0|^2 dV} \quad (4)$$

where $E_{in,QD}$ is the electric field inside the QDs in the presence of MNPs and E_0 is the electric field inside the QDs in the absence of MNPs. The integration is over the QD volume (V). $\gamma_{nr,metal}$ is the exciton transfer rate of the QD because of the energy transfer to MNP, which is calculated by²⁸

$$\gamma_{nr,metal,\alpha} = \frac{2}{\hbar} b_\alpha \left(\frac{ed_{exc}}{\epsilon_{eff}} \right)^2 \frac{R_{MNP}^3}{d^6} \left| \frac{3\epsilon_0}{2\epsilon_0 + \epsilon_{MNP}(\omega)} \right|^2 \text{Im} \left[\frac{\epsilon_{MNP}(\omega)}{\epsilon_{eff}} \right] \quad (5)$$

where $b_\alpha = 1/3, 1/3, 4/3$ for $\alpha = x, y, z$, respectively, ϵ_0 is the dielectric constant of the outside medium, $\epsilon_{MNP}(\omega)$ is the dielectric function of the MNP, R_{MNP} is the MNP radius, ed_{exc} is the exciton dipole moment in the QD, d is the center-to-center separation distance between the QDs and MNPs, and $\epsilon_{eff} = (2\epsilon_0 + \epsilon_{SQD})/3$ is the effective dielectric constant.²⁹ In the case of plasmon coupling with the quantum dots, we compute an emission enhancement factor of 2.15 for the donor QDs and 2.31 for the acceptor QDs (details are in Supporting Information: Plasmon enhanced QDs). The experimental

enhancement factor is calculated through the ratio of the PL spectral area under the curves. These results are in good agreement with the experimental values of 2.25 and 2.69 for the donor and acceptor QDs, respectively (Figure 2b).

Plasmon-Coupled FRET System. While the plasmon is coupled to donors, when we employ the acceptors in carefully designed positions, as energy transfer pairs, we observe a 1.93-fold emission enhancement of the acceptor QDs. This emission enhancement is higher compared to enhancement only due to FRET mechanism (1.30-fold). We further investigate modified PL mechanisms, through the photoluminescence lifetimes of the QD layers at the donor emission wavelength (Figure 5a). Donor QDs exhibit an amplitude averaged decay lifetime of 1.33 ns. In the presence of Au NPs (no acceptor QDs), this donor QD lifetime decreases down to 0.51 ns due to plasmon resonance energy transfer (Figure 5a, green star). In the presence of acceptors (no MNPs), the donor QD lifetime decreases to 0.62 ns due to FRET between the donor and acceptor QDs (Figure 5a, blue triangle-up). Finally, when plexitons are generated in the presence of Au NPs and acceptor QDs we observe a significant reduction in the lifetime of donor QDs to 0.29 ns showing a strong energy transfer between all species (PRET and FRET) (Figure 5a, purple triangle-down). For the plexitonic system described above (plasmon coupling to donor with FRET to acceptor), the energy transfer rate is calculated to be 2.70 ns^{-1} , which is much higher as compared to the FRET rate of 0.86 ns^{-1} without plasmon coupling (the transfer rate is calculated using $1/\tau_{(p)DA} - 1/\tau_D$).

At the acceptor QD emission wavelength, the acceptor QDs have an amplitude averaged decay lifetime of 1.53 ns as shown in Figure 5b (red square). In the presence of donors, the acceptor QD lifetime increases to 3.11 ns due to FRET between the donor and acceptor QDs (Figure 5b, blue triangle-up). Finally, in the presence of Au NPs (donor-coupled QD plexiton), we observe a significant increase in the acceptor QD lifetime from 1.53 to 3.91 ns showing a strong D–A energy transfer (Figure 5b, purple rhombic). In the control experiments, where the Au NPs is placed at sufficiently long distances (12 ML of PDDA/PSS spacing) to the acceptor quantum dots (dubbed as psA), at the same distance as in the case of plasmon-donor–acceptor case the acceptor QD is not directly influenced and their lifetime slightly decreases to 1.44 ns (Figure 5b, blue circle).

When the donor-coupled plexiton with FRET mechanism is in play (Figure 3a), the $\kappa_{D(A),DPMNRET}$ donor (acceptor) emission enhancement factor is

$$\kappa_{D,DPMNRET} = \left[\frac{A_D(\omega_{D,emiss})A_D(\omega_{laser})\gamma_{0,D,exc}}{A_D(\omega_{D,emiss})Y_{0,D}\gamma_{0,D,exc} + (1 - Y_{0,D})\gamma_{0,D,exc} + \gamma_{D,nr,metal} + \gamma_{DPMNRET}} \right] \quad (6)$$

$$\kappa_{A,DPMNRET} = \frac{A_{AD}(\omega_{A,emiss})A_{AD}(\omega_{laser})\gamma_{0,D,exc}}{A_{AD}(\omega_{D,emiss})Y_{0,A}\gamma_{0,A,exc} + (1 - Y_{0,A})\gamma_{0,A,exc} + \gamma_{A,nr,metal}} \left(1 + \frac{\gamma_{NRET}}{A_D(\omega_{D,emiss})Y_{0,D}\gamma_{0,D,exc} + (1 - Y_{0,D})\gamma_{0,D,exc} + \gamma_{D,nr,metal} + \gamma_{DPMNRET}} \frac{A_D(\omega_{laser}) I_{0,D,emiss}(\omega)}{A_{AD}(\omega_{laser}) I_{0,A,emiss}(\omega)} \right) \quad (7)$$

Table 1. Summary of the Experimental and Theoretical Analysis Results^a

Time-Resolved Analysis (Experimental)									
τ_D	τ_{D-A}	τ_{pD}	τ_{pD-A}	τ_{D-pA} (FRET)	τ_{D-pA} (no FRET)	k_{FRET}	k_{p-FRET}	η_{FRET}	η_{p-FRET}
1.33	0.62	0.51	0.29	0.67	1.31	0.86	2.70	0.53	0.78
τ_A	τ_{A-D}	τ_{pA}	τ_{pA-D}	τ_{A-pD} (FRET)	τ_{A-pD} (no FRET)	k_{FRET}	k_{p-FRET}	η_{FRET}	η_{p-FRET}
1.53	3.11	1.17	1.91	3.91	1.44				
Steady State Analysis (Experimental)									
I_D	I_{D-A}	I_{pD}	I_{pD-A}	I_{D-pA}	ζ D(FRET)	ζ pD	ζ D(pD-FRET)	ζ D(pA-FRET)	
10889	7044	24457	15735	9305	0.65	2.25	1.45	0.85	
I_A	I_{A-D}	I_{pA}	I_{pA-D}	I_{A-pD}	ζ A(FRET)	ζ pA	ζ A(pD-FRET)	ζ A(pA-FRET)	
9059	11732	24357	24455	17468	1.30	2.69	1.93	2.70	
Steady State Analysis (Theoretical)									
ζ D(FRET)			ζ pD		ζ D(pD-FRET)			ζ D(pA-FRET)	
0.54			2.15		1.30			0.74	
ζ A(FRET)			ζ pA		ζ A(pD-FRET)			ζ A(pA-FRET)	
1.46			2.31		2.80			3.37	
at donor emission wavelength	amplitude averaged lifetime (ns)		$t1$ (ns)	$t2$ (ns)	$t3$ (ns)	A1	A2	A3	
D	1.33		2.295 ± 0.034	0.566 ± 0.018	8.993 ± 0.206	5154	10986	451	
pD	0.51		7.178 ± 0.210	0.277 ± 0.006	1.396 ± 0.027	224	18368	3087	
D–A	0.62		0.304 ± 0.007	1.559 ± 0.030	6.934 ± 0.161	17919	3633	379	
pD–A	0.29		0.194 ± 0.004	1.023 ± 0.028	5.399 ± 0.225	23474	2165	157	
D–pA	0.67		8.710 ± 0.286	0.365 ± 0.009	1.754 ± 0.035	205	15770	2956	
at acceptor emission wavelength	amplitude averaged lifetime (ns)		$t1$ (ns)	$t2$ (ns)	$t3$ (ns)	A1	A2	A3	
A	1.53		6.863 ± 0.132	2.144 ± 0.031	0.638 ± 0.023	791	6046	8841	
pA	1.17		6.121 ± 0.148	1.867 ± 0.025	0.549 ± 0.017	493	5801	10332	
D–A	3.11		45.070 ± 2.800	6.630 ± 0.088	1.865 ± 0.038	42	2935	9741	
pD–A	3.91		7.295 ± 0.098	1.336 ± 0.052	28.228 ± 0.807	4025	7886	278	
D–pA	1.91		8.317 ± 0.170	2.770 ± 0.044	0.926 ± 0.028	692	4704	8605	

^a I_D : integrated donor emission intensity. I_{D-A} : integrated donor emission intensity in the case of FRET. I_{pD} : integrated donor emission intensity when plasmon is coupled to donor. I_{pD-A} : integrated donor emission intensity when plasmon is coupled to donor with FRET. I_{D-pA} : integrated donor emission intensity when plasmon is coupled to acceptor with FRET. k_{FRET} : energy transfer rate due to FRET. k_{p-FRET} : energy transfer rate due to FRET and plasmonic effects. η_{FRET} : energy transfer efficiency due to FRET. η_{p-FRET} : energy transfer efficiency due to FRET and plasmonic effects. ζ D(FRET): change in steady state photoluminescence of the donor with the energy transfer. ζ D(pD-FRET): change in steady state photoluminescence of the plasmon coupled donor with the energy transfer to acceptor. ζ D(pA-FRET): change in steady state photoluminescence of the donor with the energy transfer to plasmon coupled acceptor

where $\gamma_{0,D(A),exc}$ is the exciton recombination rate of the donor (acceptor) in the absence of MNPs at the donor side, respectively. $A_{D(A)}(\omega_{D(A),emiss(laser)})$ is the electric field enhancement factor for the donor (acceptor) due to the presence of MNPs at the donor side as a function of the donor (acceptor) emission and laser excitation frequency. $Y_{0,D(A)}$ is the donor (acceptor) quantum yield. $\gamma_{D,nr,metal}$ is the exciton transfer rate of the donor QDs because of energy transfer to the MNPs coupling only to the donor and given by eq 5. $\gamma_{DPMNRET} = \gamma_{NRET}$ is the FRET between D–A QD pair (see the Supporting Information: Plasmon Enhanced Donor QD and FRET in QDs Pair). Figure 3b presents PL intensity for the D–A QD pair when the metal NP is coupled only to the donor QD. Here, theoretically, PL intensity increases by a factor of 1.30 compared to the case without coupling to MNPs and acceptor QDs. This result is close to the experimental value of 1.45. In the case of acceptors (when the plasmon is coupled to donor), we obtain an increase of the PL intensity of 2.80, which is comparable to the experimental value of 1.93.

The photoluminescence spectra of the acceptor QDs alone and in the presence of Au MNPs show that the emission of QD film layer is increased by a factor of 2.69 under strong plasmon coupling as depicted in Figure 2b. The donor QDs are not influenced by the plasmon modes generated by Au MNPs as a result of sufficiently long separation from dielectric layers. This is also verified by time-resolved measurements for the plasmon

coupling to donor only case (dubbed as pSD). In this case, the donor QD lifetime is not considerably modified and found to be 1.31 ns (Figure 5a, dark green circle), being very close to its initial value (1.33 ns) (Figure 5a, orange square) in the control experiment, where the plasmon is separated from donor with a spacer that is the same distance as in the case of plasmon-acceptor–donor system. We can deduce that mechanisms that increase the acceptor emission are the combination of both FRET between the donor and acceptor QDs and plasmon coupling to the acceptor QD layer. In the presence of Au MNPs coupled to the acceptor QDs, we observe a 2.70-fold emission enhancement of the acceptor QDs due to plasmon coupling and FRET. In this case, we observe a significant reduction in the lifetime of the donor QDs to 0.67 ns (Figure 5a, gray rhombic), which is very close to the lifetime value of the donor QDs in the presence of the acceptor QDs and in the absence of Au MNPs (0.62 ns) (Figure 5a, blue triangle-up). The lifetime reductions are mostly due to FRET between the donor and acceptor QDs. At the acceptor QD emission wavelength, in the presence of Au MNPs coupled to the acceptor QDs the acceptor photon decay lifetime decreases from 1.53 to 1.17 ns as shown in Figure 5b (green star). Then in the presence of Au NPs (coupled to acceptor QDs only) and the donor QDs, we observe an increase in the lifetime of the acceptor QDs from 1.53 to 1.91 ns (Figure 5b, gray triangle-down). Even though there is a strong FRET mechanism taking

place between the donor and acceptor QDs, the amplitude averaged lifetime of the acceptor QDs is not increased as in the previous sample since plasmonic coupling decreases the lifetimes of QDs. For plasmon-enhanced acceptor QD and the case of FRET in QDs (Figure 4a), the emission enhancement factor for the donor and acceptor are

$$\kappa_{D,APMNET} = \frac{A_{DA}(\omega_{D,emiss})A_{DA}(\omega_{laser})\gamma_{0,D,exc}}{A_{DA}(\omega_{D,emiss})Y_{0,D}\gamma_{0,D,exc} + (1 - Y_{0,D})\gamma_{0,D,exc} + \gamma_{APMNET}} \quad (8)$$

$$\kappa_{A,DPMNET} = \frac{A_A(\omega_{A,emiss})A_A(\omega_{laser})\gamma_{0,A,exc}}{A_A(\omega_{A,emiss})Y_{0,A}\gamma_{0,A,exc} + (1 - Y_{0,A})\gamma_{0,A,exc} + \gamma_{A,nr,metal}} \quad (9)$$

Here the definition of the variables is similar to the previous cases but now the coupling is on the acceptor side (see the Supporting Information: Plasmon Enhanced Acceptor QD and FRET in QDs pair). Figure 4b shows the PL intensity for the D–A QD pair when the MNP layer is coupled only to the acceptor QD layer. We can observe a decrease in the PL intensity of 15% at the donor. The quenching observed in PL intensity is due to the energy transfer between the D and A QDs. For the acceptor case, the PL intensity is increased theoretically by 3.37 times, being similar to the experimental value of 2.70 times.

In this work, we conclude that plasmon coupling enhances nonradiative energy transfer depending on the position of the plasmon coupling. Plasmon-coupled FRET mechanism applies for the cases when the acceptor of the FRET pair is selectively plasmon-coupled, as well as when the donor of the FRET pair is selectively coupled. In both cases, our experimental results and calculations show that the enhancement in the acceptor emission with plasmon coupling to donor is significantly larger in FRET than that without plasmon coupling. The acceptor-selective plexciton is further found to lead to a higher acceptor emission enhancement than the donor-selective plexciton, as also verified by our theoretical model. However, despite the stronger acceptor emission enhancement, surprisingly, the acceptor-selective plexciton exhibits only a slight lifetime modification, unlike the case of donor-selective plexciton. This is found to stem from the opposite canceling effects on the acceptor lifetime modifications resulting from the plasmon coupling to the acceptor, which tends to increase the emission kinetics, and the FRET feeding, which tends to slow the emission kinetics. Therefore, the order of cascading FRET after PRET or PRET after FRET is indeed important.

This work also demonstrates that it is possible to gently modify the donor or the acceptor of the FRET pairs selectively through plasmonics without destroying the exciton–exciton interaction between them. Such modification of FRET mechanism with plasmonics holds great promise for FRET-driven nanophotonic device applications and FRET-based bioimaging. Selective control on the plexcitonic energy transfer will make it feasible to manipulate the detection signal and sensitivity of the desired donor or acceptor species selectively. Furthermore, in FRET studies where the energy transfer is used as the molecular ruler, this opens up the possibility to enhance the resolution of the measurement due to the enhanced energy

transfer rate either using the donor or the acceptor of interest. (Table 1 is a summary of the experimental and theoretical analysis results.)

Methods. Colloidal Synthesis of Au NPs. The first step of the Au NP synthesis involves the dissolution of 0.08 g of chloroauric acid (HAuCl₄) in 200 mL of Milli-Q water resulting in a concentration of 1 mM. Next, in a separate beaker a 44 mM solution of trisodium citrate is prepared by dissolving 0.26 g of Na₃C₆H₅O₇ in 20 mL of Milli-Q water. The first solution is then heated until it starts boiling while it is vigorously stirred. To this solution, the preheated trisodium citrate solution is added promptly. The mixture is left to boil for an additional 30 min until the red-wine-colored gold NPs solution is obtained. This synthesis results in formation of Au nanoparticles with an average diameter of 15 nm.

Colloidal Synthesis of CdTe Quantum Dots. A 0.5 L solution of 4.59 g of Cd(ClO₄)₂ and 1.31 g of thioglycolic acid (TGA) in Milli-Q water is prepared and the pH is set to 12 by adding 1 M NaOH under vigorous stirring. A second solution of 4 mL of 0.5 M H₂SO₄ is injected to 0.8 g of Al₂Te₃ and the reaction gas is transferred into the first solution with argon flow for 30 min. Quantum dots of different sizes are achieved by boiling the mixture for different durations as the increase in reaction time results in bigger QDs leading to greater (red-shifted) emission wavelength.

Layer by Layer Film Construction. To coat the negatively charged pretreated Corning glasses and to form all LbL constructions with CdTe QDs and Au NPs, a 2 mg/mL positively charged polymer solution of PDDA is prepared in a 0.1 M NaCl solution. As the complementary negatively charged polymer solution, we use PSS which is prepared at a concentration of 2 mg/mL in a 0.1 M NaCl solution.

■ ASSOCIATED CONTENT

📄 Supporting Information

Extra information on the theoretical approach and energy transfer calculations, and more experimental characterization results. This material is available free of charge via the Internet at <http://pubs.acs.org>.

■ AUTHOR INFORMATION

Corresponding Author

*E-mail: (H.V.D.) hvdemir@ntu.edu.sg, volkan@stanfordalumni.org; (Q.X.) qihua@ntu.edu.sg.

Author Contributions

†T.O. and P.L.H.-M. contributed equally to this work.

Notes

The authors declare no competing financial interest.

■ ACKNOWLEDGMENTS

The authors thank A. Govorov and Lumerical FDTD support team for their fruitful comments on the energy transfer calculations and FDTD simulations. The authors gratefully acknowledge a strong support from Singapore National Research Foundation via a Competitive Research Program (NRF-CRP-6-2010-2). Additionally, H.V.D. thankfully acknowledges Singapore National Research Foundation Fellowship Program (NRF-RF-2009-09) and the Singapore Agency for Science, Technology and Research (A*STAR) SERC (112 120 2009). Q.X. also thanks Singapore Ministry of Education via a Tier2 grant (MOE2011-T2-2-051).

■ REFERENCES

- (1) Chirico, G. *Nat. Photonics* **2009**, *3*, 81–82.
- (2) Yildiz, A.; Forkey, J. N.; McKinney, S. A.; Ha, T.; Goldman, Y. E.; Selvin, P. R. *Science* **2003**, *300*, 2061–2065.
- (3) Seker, U. O. S.; Ozel, T.; Demir, H. V. *Nano Lett.* **2011**, *11*, 1530–1539.
- (4) Farrell, D. J.; Ekins-Daukes, N. J. *Nat. Photonics* **2009**, *3*, 373–374.
- (5) Cicek, N.; Nizamoglu, S.; Ozel, T.; Mutlugun, E.; Karatay, D. U.; Lesnyak, V.; Otto, T.; Gaponik, N.; Eychmüller, A.; Demir, H. V. *Appl. Phys. Lett.* **2009**, *94*, 061105.
- (6) Lakowicz, J. R.; Ray, K.; Chowdhury, M.; Szymanski, H.; Fu, Y.; Zhang, J.; Nowaczyk, K. *Analyst* **2008**, *133*, 1308–1346.
- (7) Gaponenko, S. V. *Introduction to Nanophotonics*; Cambridge University Press: Cambridge, U.K., 2010.
- (8) Ozel, T.; Nizamoglu, S.; Sefunc, M. A.; Samarskaya, O.; Ozel, I. O.; Mutlugun, E.; Lesnyak, V.; Gaponik, N.; Eychmüller, A.; Gaponenko, S. V.; Demir, H. V. *ACS Nano* **2011**, *5*, 1328–1334.
- (9) Fedutik, Y.; Temnov, V. V.; Schops, O.; Woggon, U.; Artemyev, M. V. *Phys. Rev. Lett.* **2007**, *99*, 136802.
- (10) Ming, T.; Zhao, L.; Chen, H.; Woo, K. C.; Wang, J.; Lin, H. Q. *Nano Lett.* **2011**, *11*, 2296–2303.
- (11) Andrew, P.; Barnes, W. L. *Science* **2004**, *306*, 1002–1005.
- (12) Su, X. R.; Zhang, W.; Zhou, L.; Peng, X. N.; Pang, D. W.; Liu, S. D.; Zhou, Z. K.; Wang, Q. Q. *Appl. Phys. Lett.* **2010**, *96*, 043106.
- (13) Su, X. R.; Zhang, W.; Zhou, L.; Peng, X. N.; Wang, Q. Q. *Opt. Express* **2010**, *18*, 6516–6521.
- (14) Fofang, N. T.; Park, T. H.; Neumann, O.; Mirin, N. A.; Nordlander, P.; Halas, N. J. *Nano Lett.* **2008**, *8*, 3481–3487.
- (15) Manjavacas, A.; Garcia de Abajo, F. J.; Nordlander, P. *Nano Lett.* **2011**, *11*, 2318–2323.
- (16) Lunz, M.; Gerard, V. A.; Gun'ko, Y. K.; Lesnyak, V.; Gaponik, N.; Susha, A. S.; Rogach, A. L.; Bradley, A. L. *Nano Lett.* **2011**, *11*, 3341.
- (17) Ming, T.; Chen, H.; Jiang, R.; Li, Q.; Wang, J. *J. Phys. Chem. Lett.* **2012**, *3*, 191–202.
- (18) Zhao, L.; Ming, T.; Shao, L.; Chen, H.; Wang, J. *J. Phys. Chem. C* **2012**, *116*, 8287–8296.
- (19) Reil, F.; Hohenester, U.; Krenn, J. R.; Leitner, A. *Nano Lett.* **2008**, *8*, 4128–4133.
- (20) Cohen-Hoshen, E.; Bryant, G. W.; Pinkas, I.; Sperling, J.; Bar-Joseph, I. *Nano Lett.* **2012**, *12*, 4260–4264.
- (21) Enustun, B. V.; Turkevich, J. *J. Am. Chem. Soc.* **1963**, *85*, 3317–3328.
- (22) Gaponik, N.; Talapin, D. V.; Rogach, A. L.; Hoppe, K.; Shevchenko, E. V.; Kornowski, A.; Eychmüller, A.; Weller, H. *J. Phys. Chem. B* **2002**, *106*, 7177–7185.
- (23) Decher, G. *Science* **1997**, *277*, 1232–1237.
- (24) Soganci, I. M.; Nizamoglu, S.; Mutlugun, E.; Akin, O.; Demir, H. V. *Opt. Express* **2007**, *15*, 14289–14298.
- (25) Song, J.-H.; Atay, T.; Shi, S.; Urabe, H.; Nurmikko, A. *Nano Lett.* **2005**, *5*, 1557–1561.
- (26) Shimizu, K. T.; Woo, W. K.; Fisher, B. R.; Eisler, H. J.; Bawendi, M. G. *Phys. Rev. Lett.* **2002**, *89*, 117401.
- (27) Lakowicz, J. R. *Principles of fluorescence spectroscopy*; Springer: New York, 2006.
- (28) Govorov, A. O.; Bryant, G. W.; Zhang, W.; Skeini, T.; Lee, J.; Kotov, N. A.; Slocik, J. M.; Naik, R. R. *Nano Lett.* **2006**, *6*, 984–994.
- (29) Govorov, A. O.; Lee, J.; Kotov, N. A. *Phys. Rev. B* **2007**, *76*, 125308.